A multi-year short-range hindcast experiment for evaluating climate model moist processes from diurnal to interannual time scales

Hsi-Yen Ma[1], Chen Zhou[2], Yunyan Zhang[1], Stephen A. Klein[1], Mark D. Zelinka[1], Xue Zheng[1], Shaocheng Xie[1], Wei-Ting Chen[3], and Chien-Ming Wu[3]

5 [1]Lawrence Livermore National Laboratory, Livermore, California, USA
[2]School of Atmospheric Sciences, Nanjing University, Nanjing, China
[3]Department of Atmospheric Sciences, National Taiwan University, Taipei, Taiwan

Correspondence to: Hsi-Yen Ma (ma21@llnl.gov)

Abstract. We present a multi-year short-range hindcast experiment and its experiment procedure for better evaluating both
10 the mean state and variability of atmospheric moist processes in climate models from diurnal to interannual time scales to facilitate model development. We use the Community Earth System Model version 1 as the based model and performed a suite of 3-day long hindcasts every day starting at 00Z from 1997 to 2012. Three processes – the diurnal cycle of clouds during different cloud regimes over the Central U.S., precipitation and diabatic heating associated with the Madden-Julian Oscillation propagation, and the response of moist processes to sea surface temperature anomalies associated with the El Niño-Southern
15 Oscillation – are evaluated as examples to demonstrate how one can better utilize simulations from this experiment design to gain insights into model errors and their connection to physical parameterizations or large-scale state. This is achieved by comparing the hindcasts with corresponding long-term observations for periods based on different phenomena. These analyses can only be done through this multi-year hindcast approach to establish robust statistics of the processes under well-controlled large-scale environment. Furthermore, comparison of hindcasts to the typical simulations in climate mode with the same model
20 allows one to infer what portion of a model's climate error directly comes from fast errors in the parameterizations of moist processes. As demonstrated here, model biases in the mean state and variability associated parameterized moist processes usually develop within a few days, and manifest within weeks to affect the simulations of large-scale circulation and ultimately the climate mean state and variability. Therefore, model developers can achieve additional useful understanding of the underlying problems in model physics by conducting a multi-year hindcast experiment.

30

1 Introduction

The representation of moist processes - clouds, convection, precipitation and the associated radiative perturbations - and their interactions with the large-scale circulation in Global Climate Models (GCMs) or Earth System Models (ESMs) remains one of the grand challenges for the modeling community (Bony et al. 2015). Aside from using high resolution cloud modeling

35   (cloud-resolving models or large-eddy simulations) to study detailed cloud dynamics and physics and their interactions with large-scale environment, significant progress on process-level understanding of moist processes has also been achieved recently through the application of a climate model hindcast approach (Phillips et al. 2004; Williams et al. 2013) to gain insight relevant to the improvement of parameterizations in climate models. This progress has been made either through individual modeling studies (e.g., Xie et al. 2004, 2008; Klein et al. 2006; Barton et al. 2012, 2014; Medeiros et al. 2012; Hannah and

40   Maloney 2014; Chandra et al. 2015; Van Weverberg et al. 2015; Zheng et al. 2016; 2017; Qin et al. 2018), or through coordinated model intercomparison projects (Lin et al. 2012; Williams et al. 2013; Ma et al. 2014; Klingaman et al. 2015; Xavier et al. 2015; Morcrette et al. 2018; Ma et al. 2018; Van Weverberg et al. 2018; Chen et al. 2019).

Earlier studies with climate model hindcast experiments usually focused on a relatively short period of time, such as those

45   spanning Intensive Observation Periods or field campaigns. However, determining the robust aspects of certain cloud processes may not be achieved through these short simulations. Recent work in climate model studies has demonstrated the benefit of using multiple years of short-range hindcasts. For example, O'Brien et al. (2016) presented a direct comparison between observed and simulated weather events across multiple resolutions through the analysis of 5-day long hindcasts performed every day during a five-year period. This hindcast modeling framework allows them to assess the degree to which increased

50   resolution improves the fidelity of extreme events in the model. Further, Phillips et al. (2017) studied the land-atmosphere coupling over the U.S. Southern Great Plains (SGP) using a suite of 16 years of short-range hindcasts as well as a free-running AMIP simulation for the same period of years in comparison with the U.S. Department of Energy Atmospheric Radiation Measurement (ARM) observations. Although the surface climate state of the hindcasts deviates less from the observations in contrast to the AMIP simulation, they further identify that the model surface characteristics (e.g., vegetation cover) or physical

55   parameterizations involving land-atmosphere coupling are more important factors than the performance of surface climate state in controlling the coupling behaviors. Chen et al. (2019) assessed precipitation biases in the Community Atmosphere Model, version 5 (CAM5) during the abrupt onset of the South China Sea summer monsoon, a key precursor of the overall East Asia summer monsoon. A multi-year hindcast approach was utilized to obtain the well-constrained synoptic-scale horizontal circulation each year during the onset period. Their results highlighted the need for an appropriate representation of

60   land-ocean-convection interactions over coastal areas in order to improve the simulation of monsoon onset.

The above examples indicate the benefit of using multiple years of short-range hindcasts for robust process-level modeling studies in comparison with long-term observations. Also, evaluating ensemble short-range hindcasts with the same climate

model can complement the traditional way of conducting AMIP-type model evaluation. In the present paper, we propose a

65   multi-year short-range hindcast experiment and its experiment protocol for better evaluating both the mean state and variability of atmospheric moist processes in climate models from diurnal to interannual time scales to facilitate model development. We will demonstrate the unique value of diagnosing systematic model errors from diurnal to interannual time scales with this suite of multi-year short-range hindcasts paired with long-term observations, such as from various satellites or from major field programs like the U.S. Department of Energy ARM Program. Process-level understanding can be achieved by comparing

70   hindcasts with observations for periods based on the phenomena of interest rather than the climatological mean state. Three processes – the diurnal cycle of clouds during different cloud regimes at the ARM SGP Site, precipitation and diabatic heating associated with the Madden-Julian Oscillation (MJO), and moist processes response to sea surface temperature (SST) anomalies associated with the El Niño-Southern Oscillation (ENSO) – are evaluated as examples to gain insights into model errors and their connection to physical parameterizations. We also demonstrate that systematic errors in the mean state of moist

75   processes over the global scale are very robust and do not show significant interannual variation in either error magnitudes or patterns over large spatial domains. The remainder of this manuscript is organized into three sections. Section 2 describes the hindcast experiment design, experiments performed and validation datasets. Section 3 presents three examples of how we can better utilize this suite of multi-year short-range hindcasts to evaluate the variability of moist processes over various time scales. Section 4 present a summary.

80   ## 2 Model experiments and validation data

2.1 Model and experiment design

All simulations were conducted with the CAM5 (version cesm1_0_5, FC5 compset, Neale et al. 2012) using the finite volume dynamical core at a horizontal resolution of 0.9° latitude by 1.25° longitude and 30 vertical levels. The land model is the Community Land Model version 4.0 (CLM4) with the same horizontal resolution.

85

The hindcast procedure is based on Ma et al. (2015). We applied the horizontal velocities, temperature, specific humidity and surface pressure from the ERA-Interim Reanalysis (Dee et al. 2011) for the initial atmospheric states. A nudging simulation with CAM5/CLM4 was also performed to acquire other necessary variables (e.g., cloud and aerosol fields), which are not available from the ERA-Interim Reanalysis for the atmospheric initial conditions. The nudging simulation started from January

90   1st, 1996 and stop at December 31st, 2012 with a 6 h relaxation time scale. Land initial conditions are taken from an offline land model simulation forced by reanalysis and observations including precipitation, surface winds, and surface radiative fluxes (N. Viovy 2013, unpublished data). The offline land model simulation started from 1990 to 2012 and we performed five cycles (1990 to 2012) for the offline simulation to allow proper spin-up of the land conditions. The multi-year hindcast experiment is a suite of 3-day long hindcasts starting at 00Z every day for the years of 1997 to 2012 (Figure 1) using the initial

95   conditions obtained from the procedure described above. We concatenated each hindcast from 24-48 (48-72) hours lead time

to form a pseudo Day 2 (Day 3) time series of 16-years duration from 1997 to 2012. Day 1 data are not analyzed to minimize the impact of model spin-up (Ma et al. 2013; 2014).

We also conducted a 16-year long Atmospheric Model Intercomparison Project (AMIP, Gates 1992) simulation with the same
100   model for the same period. In this AMIP simulation, the state of the atmosphere evolves freely without constraints. Both experiments are prescribed with the National Oceanic and Atmospheric Administration (NOAA) Optimum Interpolation weekly SSTs and sea ice (Reynolds et al. 2002). To compare with high-temporal frequency observations collected at the ARM permanent sites as well as at various major field campaign locations within the simulation period, we have additionally generated output at model timestep (30 minutes interval) in additional to output for the entire global domain. Figure 2 and
105   Table 1 identify their geographical locations and output grids.

2.2 Comparison datasets

Daily global observational precipitation is adopted from the Global Precipitation Climatology Project Version 1.2 (GPCP, Adler et al. 2003). Absorbed shortwave flux at top of atmosphere (SWAbs), outgoing longwave radiation (OLR) as well as net surface shortwave and longwave fluxes are obtained from Clouds and the Earth's Radiant Energy System (CERES) Energy
110   Balanced And Filled (EBAF) observations (Loeb et al. 2009; Kato et al. 2013, Edition 2.8). Total cloud fraction is from the International Satellite Cloud Climatology Project (ISCCP) D2 dataset (Rossow et al. 1999). Global winds and surface turbulent heat fluxes are from the ERA-Interim Reanalysis. Vertical profiles of cloud fraction at the ARM SGP site are from the ARM Best Estimate (ARMBE; Xie et al. 2010) Active Remote Sensing of Clouds data (ARSCL; Clothiaux et al. 2000, 2001). The available time period of the dataset is listed in Table 2. We interpolated all the datasets onto CAM5's grid for better comparison.

115   **3 Example analysis**

Our goal here is to demonstrate the usefulness of the multi-year hindcasts in providing a different perspective on several long-standing moist processes errors in GCMs through three examples.

3.1 Cloud regimes at the ARM SGP site

One common application of hindcasts for model evaluation is during major field campaigns where intensive observations are
120   available at very high temporal scale. However, field campaigns are usually confined to a certain short period and cannot determine the robust aspects of certain cloud processes, which are available only from long-term monitoring as provided by satellites or permanent ground-based sites. From over ten years of cloud radar observations at the ARM SGP site, Zhang and Klein (2010) computed the diurnal cycle of cloud vertical structure for four distinct cloud regimes: daytime clear sky, daytime shallow convection, afternoon deep convection and nighttime convection (Figure 3 a-d). Each composite consists of
125   somewhere between 79 and 229 days spanning the warm seasons for a 10-year period. We also created the same model composites (Figure 3 e-h) from the model grid box nearest the SGP site (Figure 2), for the exact same days from the Day 2

hindcasts. We use the model cloud fraction for this comparison because the variables for using a radar simulator (Zhang et al. 2018; 2019) were not saved at the time the hindcasts were done. This analysis, which cannot be achieved as easily from the usual AMIP simulations, is a more precise way of model parameterization evaluation because it minimizes the impact of 130 erroneous large-scale states on the clouds. This is because the atmospheric large-scale state is closer to observations during each diurnal cycle of the hindcasts than it is in the AMIP simulation. Furthermore, multi-year hindcasts provide a sufficient number of events to make a meaningful comparison with observations so that conclusions from such studies are more statistically robust.

135 In Figure 3, the model overestimates high clouds regardless of cloud regime, even for clear sky condition. For clear sky condition, the model also shows middle- and low-level clouds. One possible explanation is that the deep convection scheme in the model is triggered whenever the convective available potential energy (CAPE) is larger than 70 J kg^{-1}. During the daytime in the warm seasons, CAPE is usually larger than the threshold and deep convection is easily triggered, resulting in the transport of water vapor and detrainment of cloud condensates. For the shallow convection regime, the model overestimates 140 middle-level clouds by ~4-6% but underestimates shallow clouds by ~10%. For afternoon deep convective cloud regime, the model cannot simulate the transition from shallow to deep convective clouds. The deep convection clearly starts too early from around 11 local time rather than 15 in the afternoon. Also, the model underestimates both shallow and middle-level cloud fraction by ~10%. The model completely misses the nighttime convection regime, and only shows some deep convection starting around noon. The too early afternoon convection and the lack of nocturnal convection over land are common model 145 problems as reported in previous studies (e.g., Dai 2006; Jiang et al. 2006; Covey et al. 2016). We do realize that there are already small errors in the Day 2 large-scale state and they can also contribute to the errors in the simulated cloud fields. Nevertheless, their impact is still much smaller compared to the errors due to parameterizations deficiencies.

With multi-year hindcasts and long-term cloud observations to build up robust statistics, these comparisons help identify 150 specific cloud regime deficiencies under very similar large-scale meteorological conditions, and scheme developers can further focus on improving specific processes represented in the cloud and convection parameterizations.

3.2 Model biases associated with MJO

The MJO (Madden and Julian 1971, 1972) is the dominant mode of intra-seasonal variability in the tropics. MJO has significant impacts on the global water cycle as it can interact with many weather and climate phenomena (Zhang 2013). Nevertheless, 155 contemporary GCMs still simulate poor MJO including its weak amplitude and lack of eastward propagation (Jiang et al.2015, Ahn et al. 2017). Recent studies suggest that the instability and propagation of the MJO are regulated by various feedback processes including cloud-radiation and wind-evaporation feedbacks (Sobel and Maloney 2012, 2013; Adams and Kim 2016; Ciesielski et al. 2017). These feedback processes need to be well represented in GCMs in order to produce realistic MJO. A particularly relevant process responsible for the eastward propagation of the MJO is the "pre-conditioning" process consisting

of low-level moistening and shallow convective heating structure at the eastern edge of MJO deep convection (e.g., Jiang et al. 2011; Johnson and Ciesielski 2013; Powell and Houze 2013; Xu and Rutledge 2014). This process destabilizes the environment encouraging subsequent development of deep convection.

As each MJO event is unique from one another, one can take advantage of the multi-year hindcasts to composite precipitation, winds and diabatic heating profiles (Q1, Yanai et al. 1973) based on observed MJO phases with the focus on identifying robust model biases associated with the MJO. Figure 4 present the observed composites of November to April 20-100 day band-pass filtered NOAA Interpolated Outgoing Longwave Radiation (OLR) anomalies and horizontal wind anomalies at 850mb from ERA-Interim, as a function of the eight phases of the MJO (Wheeler and Hendon 2004). The observed MJO shows a core of deep convection (center of negative OLR anomalies) over the Indian Ocean around 80°E associated with low-level convergence in winds during Phase 2. The core of deep convection slowly propagates eastward, and the intensity of OLR decreases after the core of MJO crosses over the Maritime Continent and reaches the central Pacific (Phases 6-8). Figure 5 shows composites of November to April precipitation and horizontal wind biases from Day 3 hindcasts, as well as 20-100 day band-pass filtered NOAA Interpolated OLR anomalies, as a function of the eight phases of the MJO. The observed OLR anomalies are superimposed to highlight the location of the MJO at each phase. We find that there is a dry bias in Day 3 hindcasts over the core of deep convection (center of negative OLR anomalies) associated with MJO, and a wet bias to the east over the region of suppressed convection (center of positive OLR anomalies) for all the phases as the MJO moves eastward. The dry bias is largest over Indian Ocean during Phase 2 with magnitude ~ -6 mm day^{-1}, and the wet bias is largest over western Pacific during Phase 8 with magnitude ~5-6 mm day^{-1}. The dry bias is usually attributed to the lack of organized convection in the model (Moncrieff et al. 2017), and the wet bias is consistent with the too frequently triggered deep convection scheme even under suppressed large-scale condition. Further, there is a persistent dry bias over Borneo and part of Sumatra for all the phases indicating a possible local effect of diurnal cycle of convection. The dry bias is more significant during Phase 4 and 5 as the MJO crosses over the Maritime Continent. The 850 mb winds show a biased low-level convergence near the Equator consistent with the excessive precipitation bias to the east over the region of suppressed convection.

During Phases 2 and 3 when the MJO is over the Indian Ocean, the anomalous Q1 profiles reveal that the magnitude of shallow heating is very weak (<0.4 K day^{-1}) to the east over the region of suppressed convection between 100°E and 120°E in Phase 2 and the heating is not restricted to low levels between 120°E and 150°E in Phase 3. Instead, there is an anomalous heating associated with deep convection in Phase 3, which is not evident in the observations as indicated from previous studies (Jiang et al. 2011). This suggests that the model fails to simulate the pre-conditioning moistening processes and the gradual transition from shallow to deep convection as MJO propagates. Figure 6 presents Hovmöller diagrams (longitude versus time in lag days) of rainfall anomalies along an equatorial band based on the lag correlation over an Indian Ocean box for both GPCP and Day 3 hindcasts. The model shows an eastward propagation of precipitation anomalies associated with the MJO. However, the slightly lower correlation coefficients in the hindcasts (~0.3 vs ~0.4 in observation) east of 105°E is consistent with the

weakening of MJO eastward propagation particularly over the Maritime Continent. Previous studies have identified Maritime
195   Continent as a "barrier" for MJO propagation and most MJO episodes in the models fail to propagate across it due to several
possible reasons, such as interactions of convection, clouds, surface fluxes and local circulation within a diurnal cycle, land-
sea contrast, terrain effect, or east-west low-level moisture gradient (Hagos et al. 2016; Jiang 2017; Zhang and Ling 2017).
Although further diagnosis is required to fully understand the underlying problems for MJO propagation, our analysis with
multi-year hindcasts indicates issues in the early development of biases in the shallow and deep convections associated with
200   the MJO, as well as their interactions with the diurnal cycle of convection over the Maritime Continent.

3.3 Interannual variations of moist processes

3.3.1 Variations of moist processes associated with ENSO

Being the leading mode of interannual variability in the tropics and extra-tropics, ENSO has significant impact on both regional
and global temperature, circulation, and moist processes through teleconnections. To gain insights into whether or not errors
205   in the response of these fields to SST anomalies can be attributed to parameterization errors or whether errors in the circulation
response to SST anomalies also contribute, one can further contrast the multi-year hindcasts with the behavior of a companion
AMIP simulation with the same boundary conditions (SST and sea ice). To this end, we first selected several fields to compute
their monthly anomalies and then regressed these anomalous fields onto the Nino 3.4 index. Figure 7 shows the regression
maps of precipitation, SWAbs, surface net flux (from atmosphere to the surface), and the surface zonal wind stress from
210   observations, Day 2 hindcasts and the AMIP simulation (pattern statistics are shown in Table 2). The motivation for selecting
these fields is because the tropical response of precipitation represents the atmospheric diabatic heating that forces circulation
anomalies. On the other hand, surface radiation, turbulent heat fluxes, and wind stress provide critical heat and momentum
forcings for SST anomalies and govern the ENSO behavior. The performance of these fields from an uncoupled atmospheric
GCM is considered to be highly relevant for evaluation when it couples to an ocean model (Sun et al. 2006; Guilyardi et al.
215   2009).

The responses of these fields from Day 2 hindcasts show a better agreement both in the spatial patterns and magnitude with
observations compared to the AMIP response (right column in Figure 7). This is especially evident for precipitation, absorbed
shortwave flux and zonal wind stress over the Western North Pacific, South Pacific Convergence Zone and Indian Ocean. The
remote teleconnections may be chaotic or poorly done by the model, causing a poor simulation in the AMIP mode. The
220   circulation anomalies are well constrained in the hindcasts and the response SST anomalies is much superior. This shows that
remote errors are mostly the result of poor circulation on long-term time scales although the poor circulation may be caused
by model physics in the first place and deteriorates through feedback processes with time. This is evident as there are still
biases in the hindcasts indicating problems from parameterizations in representing those response to SST changes even over
local Nino 3.4 region.

225   Surface net flux and zonal wind stress also show a greater change between hindcast and AMIP response compared to precipitation and SWAbs. It is reasonable for the latter two moist processes to show less changes as they are fast processes and the biases associated with model parameterizations usually develop within a few days of model integration (Xie et al. 2012; Ma et al. 2014). It is also reasonable for zonal wind stress to show greater change as the low-level winds are well constrained for the hindcasts. For surface net heat flux, the errors are contributed from various flux terms including radiation

230   and turbulent heat fluxes, which are affected by both model physics and dynamics. Therefore, the net heat flux shows the lowest spatial correlation and root mean square errors in both hindcasts and the AMIP simulation compared to other fields.

3.3.2 Robustness of systematic errors

One question raised from earlier studies (Xie et al. 2012 and Ma et al. 2014) of the correspondence between short- and long-time-scale errors is whether systematic errors of moist processes show significant interannual variation in the mean state biases.

235   Figure 8 shows the pattern statistics between errors from the individual annual means in the hindcasts or AMIP simulation, and errors in the 16-year mean of the AMIP simulation (the reference fields) for precipitation, total cloud fraction (from the ISCCP cloud simulator), SWAbs, and OLR. Compared to the long-term mean errors in the AMIP simulations, annual mean errors of the individual years for these fields show very similar magnitude in correlation and the normalized spatial standard deviation from the hindcasts at either time lag. This is also the case for individual AMIP years although the correlations and

240   standard deviations show slightly larger spread. Compared to Day 2 hindcasts, the correlations and standard deviations from Day 3 hindcasts are closer to those from the AMIP simulations indicating the bias growth toward the AMIP bias with hindcast lead time. We further find that the magnitude of correlations for annual mean errors between individual hindcast years and the long-term AMIP simulations are not sensitive to the ENSO phase in a given year for these fields. This is also the case if seasonal means are compared (Figures not shown here). These results suggest that mean errors in the moist processes are very

245   robust and do not show significant interannual variations. Indeed, averaging the hindcast errors over many years (indicated by "2" or "3" in Figure 8) only slightly improves the agreement with the AMIP reference field. Thus, one can identify robust model errors in the mean state from only one year of hindcasts with enough ensemble members. A similar conclusion with multiple years of short AMIP-type simulations was also suggested by Wan et al. (2014). These results suggest that relatively short simulations will be effective at reducing the systematic moist process errors of a very high-resolution climate model

250   which is too expensive to regularly perform multi-year simulations.

It is also of interest to compare the absolute magnitude of errors in individual years to that of the long-term systematic error in the AMIP simulation. To do so, we calculated the annually cloud error metrics proposed in Klein et al. (2013) in Figure 9. These metrics are scalar measures of performance in simulating the space-time distribution of several cloud measures, with

255   better performance indicated by smaller E values. It is not surprising that the hindcasts show better performance in all the cloud metrics as the large-scale circulation and state are not too far from the reanalysis. This is also true for the interannual variations in global mean cloud radiative effect at the top of the atmosphere (Figure 10). We find that all the metrics and the cloud

radiative effect show interannual variations indicating that the circulation and state anomalies make a significant contribution to interannual variations although these metrics or errors in the cloud radiative effect are not sensitive to ENSO phase. We

260   further find that there is a larger difference between hindcasts and AMIP in the total cloud amount error metric (E_{TCA}) implying that errors in the large-scale circulation and state make a larger contribution to errors in E_{TCA} than cloud radiative properties (Figure 10).

4 Summary

In this study, we propose a multi-year short-range hindcast experiment and its experiment protocol for better evaluating both

265   the mean state and variability of atmospheric moist processes in climate models from diurnal to interannual time scales to facilitate model development. We also demonstrate that one can obtain unique understanding into robust GCM systematic moist processes errors by diagnosing these processes with corresponding observations for periods based on different phenomena. The present study also demonstrates that it is now feasible to systematically evaluate climate model moist processes in deterministic weather-prediction mode just as the moist processes in weather prediction models are often evaluated

270   in analyses or re-analyses (Jakob 1999, Yang et al. 2006).

Three processes – the diurnal cycle of clouds during different cloud regimes at the ARM SGP Site, precipitation and diabatic heating associated with the MJO, and the response of moist processes to ENSO SST anomalies – are evaluated as examples of using this multi-year hindcast experiment to gain insights into robust model errors and their connection to physical

275   parameterizations and large-scale state. These analyses can only be done through the hindcast approach to establish robust statistics of the processes under well-controlled large-scale environment. These comparisons identify specific model deficiencies that subsequent parameterization development should focus on. The proposed experiment and evaluation method also complement the existing ways of climate model evaluation, such as performing GCM simulations in the AMIP mode. Results from the multi-year hindcasts also suggest that systematic errors in the mean state of moist processes are very robust

280   and do not show significant interannual variation in error magnitude or patterns over large spatial domain.

In addition to processes indicated above, further studies on monsoon variability (e.g., South American and Asian monsoons, Chen et al. 2019), land-atmosphere interactions (Phillips et al. 2017), or detailed MJO studies with longer hindcast duration (Klingaman et al. 2015), are currently being explored with these hindcasts. Indeed, GCMs usually perform more poorly for

285   climate variability than for mean state. As demonstrated in previous studies and here, model mean biases associated parameterized moist processes usually develop within a few days and manifest within weeks to affect the simulations of large-scale circulation and ultimately the climate mean state and variability. Therefore, model developers can achieve useful understanding of the underlying problems in model physics by conducting multiple years of hindcasts as demonstrated in the present work. Although newer version of the CAM and CLM is now available (CAM6/CLM5), similar systematic errors

290   associated with moist processes remain present in the latest model version. Therefore, it is still worthwhile to study these

hindcasts. In the meantime, we also plan to conduct another suite of multi-year hindcasts with the latest DOE Exascale Energy Earth System Model (E3SM, Golaz et al. 2019). The hindcasts will also be available to the community once available.

295 Finally, the multi-year hindcast approach presented in this study is also intended as one of the experiment protocols which will be used in the Diurnal Cycle of Precipitation (DCP, https://portal.nersc.gov/cfs/capt/diurnal/) model intercomparison project under the Global Energy and Water cycle Exchanges (GEWEX) Global Atmospheric System Studies (GASS). This project is aimed to understand what processes control the diurnal and sub-diurnal variation of precipitation over different climate regimes in observations and in models. The project will also identify the deficiencies and missing physics in current GCMs to gain insights for further improving the parameterization of convection.

300 **Code and data availability**

The model code is the CESM1 (cesm1_0_5, FC5 compset, F09_F09 resolution) and is available over http://www.cesm.ucar.edu/models/cesm1.0/. All model necessary input files are available over https://svn-ccsm-inputdata.cgd.ucar.edu/trunk/inputdata/. The boundary conditions of SST and sea ice data are available over https://www.esrl.noaa.gov/psd/data/gridded/data.noaa.oisst.v2.html, The simulations is available online through the NERSC

305 Science Gateways (https://portal.nersc.gov/archive/home/h/hyma/www/CAPT/CAPT_Long). An detailed documentation for this experiment and variable list is over https://portal.nersc.gov/archive/home/h/hyma/www/CAPT/CAPT_Long/CAPT_Long_output_cesm1_0_5_v5.pdf.

Author contribution

HM designed, performed, analyzed the experiments, and wrote the first draft of the manuscript. SK and SX contributed to the

310 design of the experiments and to the interpretation of the results. CZ, YZ, MZ, and XZ contributed to the analysis of experiments, and the interpretation of the results. WC, and CW contributed to the interpretation of the results. All coauthors contributed to the manuscript text.

Acknowledgments

This study was funded by the U.S. Department of Energy (DOE) Regional and Global Model Analysis program area, and the

315 Atmospheric System Research and Atmospheric Radiation Measurement Programs. This work was performed under the auspices of the U.S. DOE by LLNL under contract DE-AC52-07NA27344.

References

Adler, R. F., Huffman, G. J., Chang, A., Ferraro, R., Xie, P.-P., Janowiak, J., Rudolf, B., Schneider, U., Curtis, S., Bolvin, D., Gruber, A., Susskind, J., Arkin, P., and Nelkin, E.: The version-2 Global Precipitation Climatology Project (GPCP) monthly precipitation analysis (1979-present), J. Hydrometeorol., 4, 1147-1167, 2003.

Ahn, M.-S., Kim, D., Sperber, K. R., Kang, I.-S., Maloney, E., Waliser, D., and Hendon, H.: MJO simulation in CMIP5 climate models: MJO skill metrics and process-oriented diagnosis, Clim. Dyn., https://doi.org/10.1007/s00382-017-3558-4, 1-23, 2017.

Barton, N. P., Klein, S. A., Boyle, J. S., and Zhang, Y.: Arctic synoptic regimes: Comparing domain-wide Arctic cloud observations with CAM4 and CAM5 during similar dynamics, J. Geophys. Res., 117, D15205, https://doi.org/10.1029/2012JD017589, 2012.

Barton, N. P., Klein, S. A., and Boyle, J. S.: On the contribution of longwave radiation to global climate model biases in Arctic lower tropospheric stability, J. Climate, 27, 7250-7269, https://doi.org/10.1175/JCLI-D-14-00126.1, 2014.

Bony, S., Stevens, B., Frierson, D. M. W., Jakob, C., Kageyama, M., Pincus, R., Shepherd, T. G., Sherwood, S. C., Siebesma, A. P., Sobel, A. H., Watanabe, M., and Webb, M. J.: Clouds, circulation and climate sensitivity, Nat. Geosci., 8, 261–268. https://doi.org/10.1038/NGEO2398, 2015.

Ciesielski, P. E., Johnson, R. H., Jiang, X., Zhang, Y., and Xie, S.: Relationships between radiation, clouds, and convection during DYNAMO, J. Geophys. Res. Atmos., 122, 2529–2548, https://doi.org/10.1002/2016JD025965, 2017.

Chen, W.-T., Wu, C.-M., and Ma, H.-Y.: Evaluating the bias of South China Sea summer monsoon precipitation associated with fast physical processes using climate model hindcast approach, J. Climate, 32, 4491–4507, https://doi.org/10.1175/JCLI-D-18-0660.1, 2019.

Clothiaux, E. E., Ackerman, T. P., Mace, G. G., Moran, K. P., Marchand, R. T., Miller, M., and Martner, B. E.: Objective determination of cloud heights and radar reflectivities using a combination of active remote sensors at the ARM CART sites, J. Appl. Meteor., 39, 645–665, 2000.

Clothiaux, E. E., Miller, M. A., Perez, R. C., Turner, D. D., Moran, K. P., Martner, B. E., Ackerman, T. P., Mace, G. G., Marchand, R. T., Widener, K. B., Rodriguez, D. J., Uttal, T., Mather, J. H., Flynn, C. J., Gaustad, K. L., and Ermold, B.: The ARM millimeter wave cloud radars (MMCRs) and the active remote sensing of clouds (ARSCL) value added product (VAP), U.S. Department of Energy Tech. Memo. ARM VAP-002.1, 56 pp, 2001.

Chandra, A. S., Zhang, C., Klein, S. A., and Ma, H.-Y.: Low-cloud characteristics over the tropical western Pacific from ARM observations and CAM5 simulations, J. Geophys. Res. Atmos., 120, https://doi.org/10.1002/2015JD023369, 2015.

Covey, C., Gleckler, P. J., Doutriaux, C., Williams, D. N., Dai, A., Fasullo, J., Trenberth, K., and Berg, A.: Metrics for diurnal cycle of precipitation: Toward routine benchmarks for climate models, J. of Climate, 29, 4461-4471, 2016.

Dai, A.: Precipitation characteristics in eighteen coupled climate models, J. of Climate, 19, 4605-4630, 2006.

Dee, D. P., Uppala, S. M., Simmons, A. J., Berrisford, P., Poli, P, Kobayashi, S., Andrae, U., Balmaseda, M. A., Balsamo, G.,
350   Bauer, P., Bechtold, P., Beljaars, A. C. M., van de Berg, L., Bidlot, J., Bormann, N., Delsol, C., Dragani, R., Fuentes, M.,
Geer, A. J., Haimberger, L., Healy, S. B., Hersbach, H., Hólm, E. V., Isaksen, L., Kallberg, P., Köhler, M., Matricardi, M.,
McNally, A. P., Monge-Sanz, B. M., Morcrette, J.-J., Park, B.-K., Peubey, C., de Rosnay, P., Tavolato, C., Thépaut, J.-N., and
Vitart, F.: The ERA-Interim reanalysis: configuration and performance of the data assimilation system, Q. J. R. Meteorol. Soc.,
137, 553–597, 2011.

355   Gates, W. L.: AMIP: The Atmospheric Model Intercomparison Project, Bull. Amer. Meteor. Soc., 73, 1962–1970, 1992.
Golaz, J.-C., Caldwell, P. M., Van Roekel, L. P., Petersen, M. R., Tang, Q., Wolfe, J. D., et al: The DOE E3SM coupled model
version 1: Overview and evaluation at standard resolution. Journal of Advances in Modeling Earth Systems, 11.
https://doi.org/10.1029/2018MS001603, 2019.
Guilyardi, E., Wittenberg, A., Fedorov, A., Collins, M., Wang, C., Capotondi, A., van Oldenborgh, G. J., and Stockdale, T.:
360   Understanding El Niño in ocean-atmosphere general circulation models, Bull. Amer. Met. Soc., 90, 325–340, 2009.
Hagos, S. M., Zhang, C., Feng, Z., Burleyson, C. D., DeMott, C., Kerns, B., Benedict, J., and Martini, M.: The impact of the
diurnal cycle on the propagation of Madden-Julian Oscillation convection across the Maritime Continent, J. Adv. Model. Earth
Syst., 8, 1552-1564. https://doi.org/10.1002/2016MS000725, 2016.
Hannah, W. M., and Maloney, E. D.: The moist static energy budget in NCAR CAM5 hindcasts during DYNAMO, J. Adv.
365   Model. Earth Syst., 6(2), 420–440, 2014.
Jakob, C.: Cloud cover in the ECMWF reanalysis, J. Climate, 12, 947–959, 1999.
Jiang, X., Lau, N.-C., and Klein, S. A.: Role of eastward propagating convection systems in the diurnal cycle and seasonal
mean of summertime rainfall over the U.S. Great Plains, Geophys. Res. Lett., 33, L19809,
https://doi.org/10.1029/2006GL027022, 2006.
370   Jiang, X., Waliser, D. E., Olson, W. S., Tao, W.-K., L'Ecuyer, T. S., Shige, S., Li, K.-F., Yung, Y. L., Lang, S., and Takayabu,
Y. N.: Vertical diabatic heating structure of the MJO: Intercomparison between recent reanalyses and TRMM estimates, Mon.
Wea. Rev., 139, 3208-3223, 2011.
Jiang, X., Waliser, D. E., Xavier, P. K., Petch, J., Klingaman, N. P., Woolnough, S. J., Guan, B., Bellon, G., Crueger, T.,
DeMott, C., Hannay, C., Lin, H., Hu, W., Kim, D., Lappen, C.-L., Lu, M.-M., Ma, H.-Y., Miyakawa, T., Ridout, J. A.,
375   Schubert, S. D., Scinocca, J., Seo, K.-H., Shindo, E., Song, X., Stan, C., Tseng, W.-L., Wang, W., Wu, T., Wu, X.,
Wyser, K., Zhang, G. J., Zhu, H.: Vertical structure and physical processes of the Madden-Julian oscillation: Exploring key
model physics in climate simulations, J. Geophys. Res. Atmos., 120, 4718-4748, https://doi.org/10.1002/2014JD022375, 2015.
Jiang, X.: Key processes for the eastward propagation of the Madden-Julian Oscillation based on multimodel simulations, J.
Geophys. Res. Atmos., https://doi.org/10.1002/2016JD025955, 2017.
380   Johnson, R. H. and P. E. Ciesielski (2013), Structure and Properties of Madden–Julian Oscillations Deduced from DYNAMO
Sounding Arrays. J. Atmos. Sci., 70, 3157-3179, https://doi.org/10.1175/JAS-D-13-065.1, 2013.

Kato, S., Loeb, N. G., Fred, F. G., Doelling, D. R., Rutan, D. A., Caldwell, T. E., Yu, L., Weller, R. A.: Surface irradiances consistent with CERES-derived top-of-atmosphere shortwave and longwave irradiances, J. of Climate, 26(9), 2719-2740. http://dx.doi.org/10.1175/JCLI-D-12-00436.1, 2013.

385 Klingaman, N. P., Woolnough, S. J., Jiang, X., Waliser, D., Xavier, P. K., Petch, J., Caian, M., Hannay, C., Kim, D., Ma, H.-Y., Merryfield, W. J., Miyakawa, T., Pritchard, M., Ridout, J. A., Roehrig, R., Shindo, E., Vitart, F., Wang, H., Cavanaugh, N. R., Mapes, B. E., Shelly, A., and Zhang, G. J.: Vertical structure and physical processes of the Madden–Julian oscillation: Linking hindcast fidelity to simulated diabatic heating and moistening, J. Geophys. Res.-Atmos., 120, 4690–4717, https://doi.org/10.1002/2014JD022374, 2015.

390 Klein, S. A., Jiang, X., Boyle, J. S., Malyshev, S., and Xie, S.: Diagnosis of the summertime warm and dry bias over the U.S. Southern Great Plains in the GFDL climate model using a weather forecasting approach. Geophys. Res. Lett., 33, L18805, https://doi.org/10.1029/2006GL027567, 2006.

Klein, S. A., Zhang, Y., Zelinka, M. D., Pincus, R., Boyle, J. S., and Gleckler, P. J: Are climate model simulations of clouds improving? An evaluation using the ISCCP simulator, J. Geophys. Res.,118, https://doi.org/10.1002/jgrd.50141, 2013.

395 Lin, Y., Donner, L. J., Petch, J., Bechtold, P., Boyle J. S., Klein, S. A., Komori, T., Wapler, K., Willett, M., Xie, X., Zhao, M., Xie, S., McFarlane, S. A., and Schumacher, C.: TWP-ICE global atmospheric model intercomparison: convection responsiveness and resolution impact, J. Geophys. Res., https://doi.org/10.1029/2011JD017018, 2012.

Loeb, G. N., Wielicki, B. A., Doelling, D. R., Smith, G. L., Keyes, D. F., Kato, S., Manalo-Smith, N., and Wong, T.: Toward optimal closure of the Earth's top-of-atmosphere radiation budget, J. Climate, 22, 748–766,
400 https://doi.org/10.1175/2008JCLI2637.1, 2009.

Ma, H.-Y., Xie, S., Boyle, J. S., Klein, S. A., and Zhang, Y.: Metrics and diagnostics for precipitation-related processes in climate model short-range hindcasts, J. Climate, 26, 1516–1534, 2013.

Ma, H. Y., Xie, S., Klein, S. A., Williams, K. D., Boyle, J. S., Bony, S., Douville, H., Fermepin, S., Medeiros, B., Tyteca, S., and Watanabe, M.: On the correspondence between mean fore- cast errors and climate errors in CMIP5 models, J. Climate,
405 27, 1781–1798, 2014.

Ma, H.-Y., Chuang, C. C., Klein, S. A., Lo, M.-H., Zhang, Y., Xie, S., Zheng, X., Ma, P.-L., Zhang, Y., and Phillips, T. J.: An improved hindcast approach for evaluation and diagnosis of physical processes in global climate models, J. Adv. Model. Earth Syst., 7, 1810–1827, https://doi.org/10.1002/2015MS000490, 2015.

Ma, H. Y., Klein, S. A., Xie, S., Zhang, C., Tang, S., Tang, Q., Morcrette, C. J., Van Weverberg, K., Petch, J., Ahlgrimm, M.,
410 Berg, L. K., Cheruy, F., Cole, J., Forbes, R., Gustafson Jr., W. I., Huang, M., Liu, Y., Merryfield, W., Qian, Y., Roehrig, R., and Wang, Y.-C.: CAUSES: On the role of surface energy budget errors to the warm surface air temperature error over the Cen- tral United States, J. Geophys. Res.-Atmos., 123, 2888–2909, https://doi.org/10.1002/2017JD027194, 2018.

Madden, R. A., and Julian, P. R.: Detection of a 40- 50 day oscillation in the zonal wind in the tropical Pacific, J. Atmos. Sci., 28, 702–708, 1971.

415   Madden, R. A., and Julian, P. R.: Description of global-scale circulation cells in the tropics with a 40-50 day period, J. Atmos. Sci., 29, 1109–1123, 1972.

Medeiros, B., Williamson, D. L., Hannay, C., Olson, J. G.: Southeast Pacific stratocumulus in the Community Atmosphere Model, J. Climate, 25, 6175–6192, 2012.

Moncrieff, M. W., Liu, C., and Bogenschutz, P.: Simulation, modeling, and dynamically based parameterization of organized
420   tropical convection for global climate models, J. Atmos. Sci., 74, 1363–1380, 2017.

Morcrette, C. J., Van Weverberg, K., Ma, H. Y., Ahlgrimm, M., Bazile, E., Berg, L. K., Cheng, A., Cheruy, F., Cole, J., Forbes, R., and Gustafson Jr., W. I.: Introduction to CAUSES: Description of weather and climate models and their near- surface temperature errors in 5 day hindcasts near the South- ern Great Plains, J. Geophys. Res.-Atmos., 123, 2655–2683, https://doi.org/10.1002/2017JD027199, 2018.

425   Neale, R. B., Chen, C. C., Gettelman, A., Lauritzen, P. H., Park, S., Williamson, D. L., Conley, A. J., Garcia, R., Kinnison, D., Lamarque, J. F., and Marsh, D.: Description of the NCAR community atmosphere model (CAM 5.0), NCAR Tech. Note NCAR/TN-486+ STR, 2010.

O'Brien, T. A., Collins, W. D., Kashinath, K., Rübel, O., Byna, S., Gu, J., Krishnan, H., and Ullrich, P. A.: Resolution dependence of precipitation statistical fidelity in hindcast simulations, J. Adv. Model. Earth Syst., 8, 976–990,
430   https://doi.org/10.1002/2016MS000671, 2016.

Phillips, T. J., Potter, G. L., Williamson, D. L., Cederwall, R. T., Boyle, J. S., Fiorino, M., Hnilo, J. J., Olson, J. G., Xie, S., and Yio, J. J.: Evaluating parameterizations in general circulation models: Climate simulation meets weather prediction. Bull. Amer. Meteor. Soc., 85, 1903–1915, 2004.

Phillips, T. J., Klein, S. A., Ma, H.-Y., Tang, Q., Xie, S., Williams, I. N., Santanello, J. A., Cook, D. R., and Torn, M. S.: Using
435   ARM Observations to Evaluate Climate Model Simulations of Land-Atmosphere Coupling on the U.S. Southern Great Plains, J. Geophys. Res., Atmos., 122, 11,524–11,548. https://doi.org/10.1002/2017JD027141, 2017.

Powell, S. W. and Houze, R. A.: The cloud population and onset of the Madden-Julian Oscillation over the Indian Ocean during DYNAMO-AMIE, J. Geophys. Res., Atmos., 118, https://doi.org/10.1002/2013JD020421, 2013.

Reynolds, R. W., Rayner, N. A., Smith, T. M., Stokes, D. C., and Wang, W.: An improved in situ and satellite SST analysis
440   for climate, J. Climate, 15, 1609-1625, 2002.

Rossow, W. B., and Schiffer, R. A.: Advances in Understanding Clouds from ISCCP, Bull. Amer. Meteor. Soc., 80, 2261–2288, 1999.

Sun, D.-Z., Thang, T., Covey, C., Klein, S. A., Collins, W. D., Hack, J. J., Kiehl, J. T., Meehl, G. A., Held, I. M., and Suarez, M.: Radiative and dynamical feedbacks over the equatorial cold tongue: Results from nine atmospheric GCMs, J. Climate, 19,
445   4059–4074, 2006.

Van Weverberg, K., Morcrette, C. J., Ma, H.-Y., Klein, S. A. and Petch, J. C.: Using regime analysis to identify the contribution of clouds to surface temperature errors in weather and climate models, Q. J. R. Meteorol. Soc., https://doi.org/10.1002/qj.2603, 2015.

Van Weverberg, K., Morcrette, C. J., Petch, J., Klein, S. A., Ma, H. Y., Zhang, C., Xie, S., Tang, Q., Gustafson Jr., W. I., Qian,
450 Y., and Berg, L. K.: CAUSES: Attribution of surface radia- tion biases in NWP and climate models near the U.S. South- ern
Great Plains, J. Geophys. Res.-Atmos., 123, 3612–3644, https://doi.org/10.1002/2017JD027188, 2018.

Xavier, P. K., Petch, J. C., Klingaman, N. P., Woolnough, S. J., Jiang, X., Waliser, D. E., Caian, M., Cole, J., Hagos, S. M.,
Han- nay, C., and Kim, D.: Vertical structure and physical processes of the Madden-Julian Oscillation: Biases and uncertainties
at short range, J. Geophys. Res.-Atmos., 120, 4749–4763, https://doi.org/10.1002/2014JD022718, 2015.

455 Xu, W., and Rutledge, S. A.: Convective characteristics of the Madden–Julian Oscillation over the Central Indian Ocean
observed by shipborne radar during DYNAMO, J. Atmos. Sci., 71, 2859-2877, 2014.

Wan, H., Rasch, P. J., Zhang, K., Qian, Y., Yan, H., and Zhao, C.: Short ensembles: An efficient method for discerning climate-
relevant sensitivities in atmospheric general circulation models, Geosci. Model Dev., 7(5), 1961–1977,
https://doi.org/10.5194/gmd-7-1961-2014, 2014.

460 Wheeler, M. C., and Hendon, H. H.: An all-season real-time multivariate MJO index: Development of an index for monitoring
and prediction, Mon. Weather Rev., 132, 1917–1932, 2004.

Williams, K. D., Bodas-Salcedo, A., Déqué, M., Fermepin, S., Medeiros, B., Watanabe, M., Jakob, C., Klein, S. A., Senior, C.
A., and Williamson, D. L.: The Transpose-AMIP II Experiment and Its Application to the Understanding of Southern Ocean
Cloud Biases in Climate Models, J. Climate, 26, 3258–3274, 2013.

465 Xie, S., Zhang, M. H., Boyle, J. S., Cederwall, R. T., Potter, G. L., and Lin, W. Y.: Impact of a revised convective triggering
mechanism on CAM2 model simulations: results from short-range weather forecasts, J. Geophys. Res., 109, D14102,
https://doi.org/10.1029/2004JD004692, 2004.

Xie, S., Boyle, J. S., Klein, S. A., Liu, X. and Ghan, S.: Simulations of Arctic mixed-phase clouds in forecasts with CAM3
and AM2 for M-PACE, J. Geophys. Res., 113, D04211, https://doi.org/10.1029/2007JD009225, 2008.

470 Xie, S. C., McCoy, R. B., Klein, S. A., Cederwall, R. T., Wiscombe, W. J., Clothiaux, E. E., Gaustad, K. L., Golaz, J. C., Hall,
S. D., Jensen, M. P., Johnson, K. L., Lin, Y. L., Long, C. N., Mather, J. H., McCord, R. A., McFarlane, S. A., Palanisamy, G.,
Shi, Y., and Turner, D. D. D.: Arm Climate Modeling Best Estimate Data a New Data Product for Climate Studies, B. Am.
Meteorol. Soc., 91, 13–20, https://doi.org/10.1175/2009bams2891.1, 2010.

Xie, S., Ma, H.-Y., Boyle, J. S., Klein, S. A., and Zhang, Y.: On the correspondence between short- and long- timescale
475 systematic errors in CAM4/CAM5 for the Years of Tropical Convection, J. Climate, 25, 7937–7955, 2012.

Yang, F., Pan, H., Krueger, S. K., Moorthi, S., and Lord, S. J.: Evaluation of the NCEP Global Forecast System at the ARM
SGP site, Mon. Wea. Rev., 134, 3668–3690, 2006.

Yanai, M., Esbensen, S., and Chu, J.–H.: Determination of bulk properties of tropical cloud clusters from large-scale heat and
moisture budgets, J. Atmos. Sci., 30, 611–627, 1973.

480 Zhang, C.: Madden–Julian Oscillation: Bridging weather and climate, Bull. Am. Meteorol. Soc., 94, 1849-1870,
https://doi.org/10.1175/bams-d-12-00026.1, 2013.

Zhang, C. and Ling, J.: Barrier effect of the Indo-Pacific Maritime Continent on the MJO: Perspectives from tracking MJO precipitation, J. Climate, 30, 3439–3459, 2017.

Zhang, Y., and Klein, S. A.: Mechanisms affecting the transition from shallow to deep convection over land: Inferences from observations of the diurnal cycle collected at the ARM Southern Great Plains Site, J. Atmos. Sci., 67, 2943–2959, 2010.

Zhang, Y., Xie, S., Klein, S. A., Marchand, R., Kollias, P., Clothiaux, E. E., Lin, W., Johnson, K., Swales, D., Bodas-Salcedo, A., Tang, S., Haynes, J. M., Collis, S., Jensen, M., Bharadwaj, N., Hardin, J., and Isom, B.: The ARM cloud radar simulator for global climate models: Bridging field data and climate models, Bull. Amer. Met. Soc., 99, 21–26, https://doi.org/10.1175/BAMS-D-16-0258.1, 2018.

Zhang, Y., Xie, S., Lin, W., Klein, S. A., Zelinka, M. D., Ma, P.-L., Rasch, P. J., Qian, Y., Tang, Q., and Ma, H.-Y.: Evaluation of clouds in version 1 of E3SM Atmosphere Model with satellite simulators, J. Adv. Model. Earth Syst., 11, https://doi.org/10.1029/2018MS001562, 2019.

Zheng, X., Klein, S. A., Ma, H.-Y., Bogenschutz, P., Gettelman, A. and Larson, V. E.: Assessment of marine boundary layer cloud simulations in the Community Atmosphere Model with Cloud Layers Unified By Binormals and updated microphysics scheme based on ARM observations from the Azores, J. Geophys. Res.-Atm., 121, 8472–8492, https://doi.org/10.1002/2016JD025274, 2016.

Zheng, X., Klein, S. A., Ma, H.-Y., Caldwell, P. M., Larson, V. E., Gettelman, A., and Bogenschutz, P.: A cloudy planetary boundary layer oscillation arising from the coupling of turbulence with precipitation in climate simulations, J. Adv. Model. Earth Syst., 9, 1973–1993, https://doi.org/10.1002/2017MS000993, 2017.

Table 1: Locations of model patch/site output associated with major field campaigns or DOE ARM sites.

Locations	Longitude	Latitude	grids
1.Niamey-1	357E-359E	14N-17N	10
2.Niamey-2	0-9E	5N-18N	120
3.DYNAMO	70E-83E	10S-9N	231
4.China-Shouxian	114E-119E	31N-34N	25
5.Darwin	129E-133E	14S-10S	20
6.Manus	146E-149E	4S-1S	12
7.Nauru	166E-169E	2S-1N	15
8.SHEBA	190E-220E	74N-78N	125
9.MAGIC-1	201E-214E	16N-25N	121
10.MAGIC-2	207E-232E	24N-30N	147
11.MAGIC-3	221E-243E	29N-36N	162
12.NSA	202E-206E	70N-73N	16
13.CARE	238E-240E	37N-39N	9
14.SGP	261E-264E	35N-38N	12
15.Vocals	272E-291E	23S-17S	112
16.Amazonia	296E-301E	13S-9S	25
17.Manaus	298E-302E	5S-1S	25
18.Azores-Graciosa	329E-334E	38N-41N	20
19.Barbados	291E-301E	10N-20N	108

520

525

Table 2: List of observation datasets.

Observations	Analyzed period	References
GPCP Precipitation V1.2	1997-2012	Adler et al. 2003
CERES EBAF Radiation Edition 2.8	2000-2012	Loeb et al. 2009; Kato et al. 2013
ISCCP D2 Cloud	1997-2009	Rossow et al. 1999
ERA-Interim Reanalysis	1997-2012	Dee et al. 2011
ARMBE ARSCL Cloud	1997-2007	Xie et al. 2010; Clothiaux et al. 2000, 2001

530

535
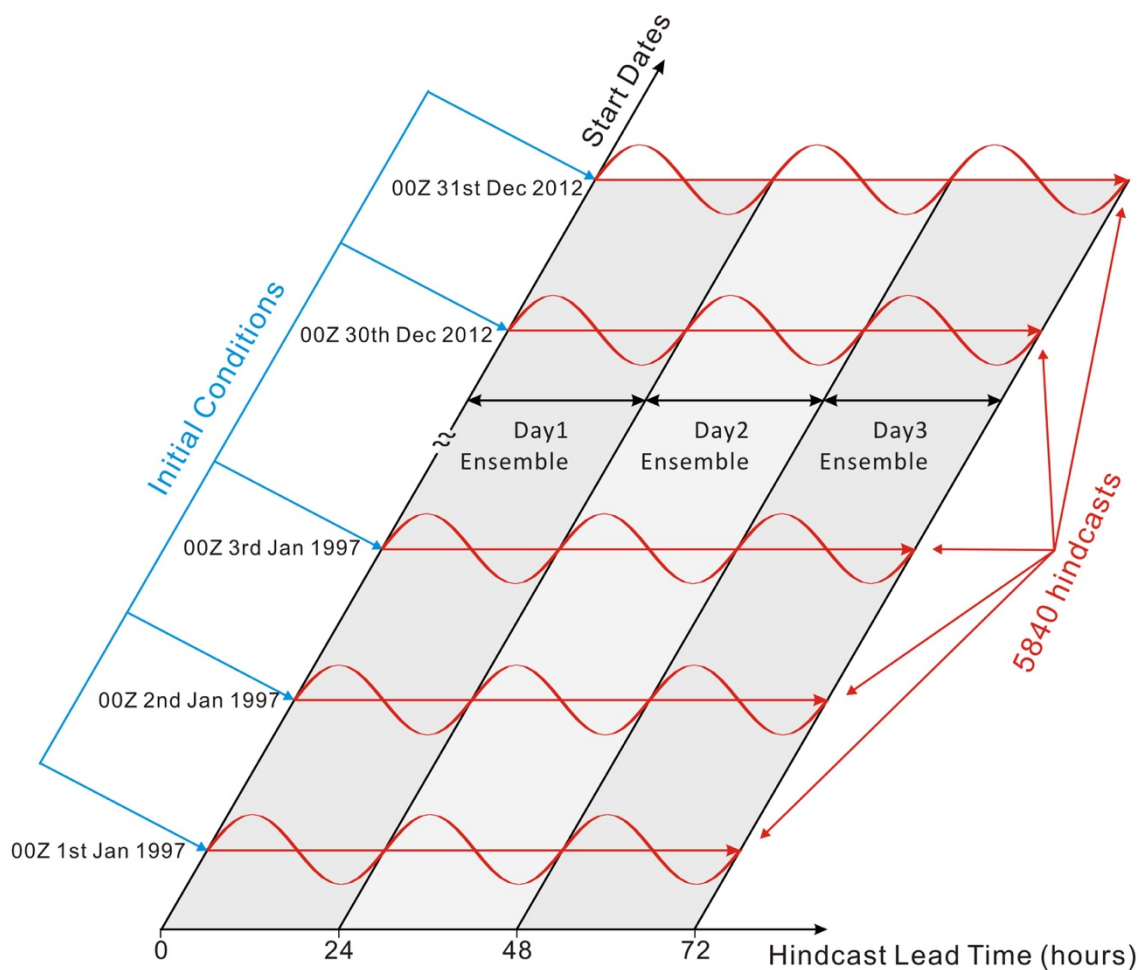
Figure 1: Schematic diagram for the multi-year hindcast procedure (modified from Ma et al. 2015) applied to series of three-day hindcasts from 1997 to 2012. Each hindcast is initialized with ERA Interim Reanalysis and the starting time is 00Z every day.

Figure 2: Locations of model patch/site output associated with major field campaigns or U.S. Department of Energy Atmospheric Radiation Measurement (ARM) sites. See Table 1 for detailed longitude and latitude information.
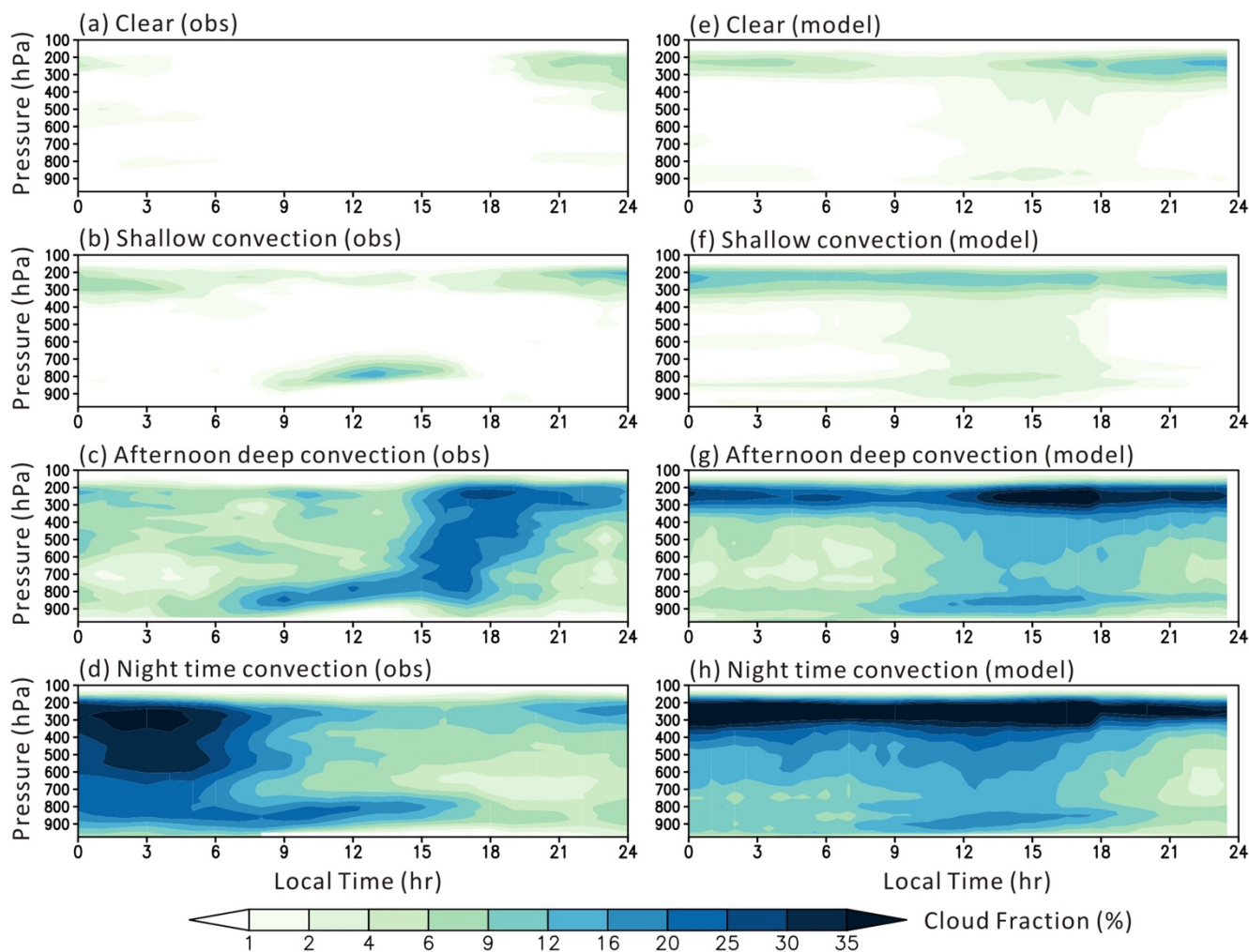
Figure 3: Diurnal cycle of cloud fraction composites (%) from May to August in the years of 1997 to 2007 from (a)–(d) ARMBE ARSCL and (e)-(h) CAPT Day 2 hindcasts for different convection regimes: (a)(e) clear-sky regime, (b)(f) fair-weather shallow cumulus regime, (c)(g) late-afternoon deep convection regime, and (d)(h) nighttime deep convection regime. Figures (a)-(d) were modified from Figure 3 in Zhang and Klein (2010).
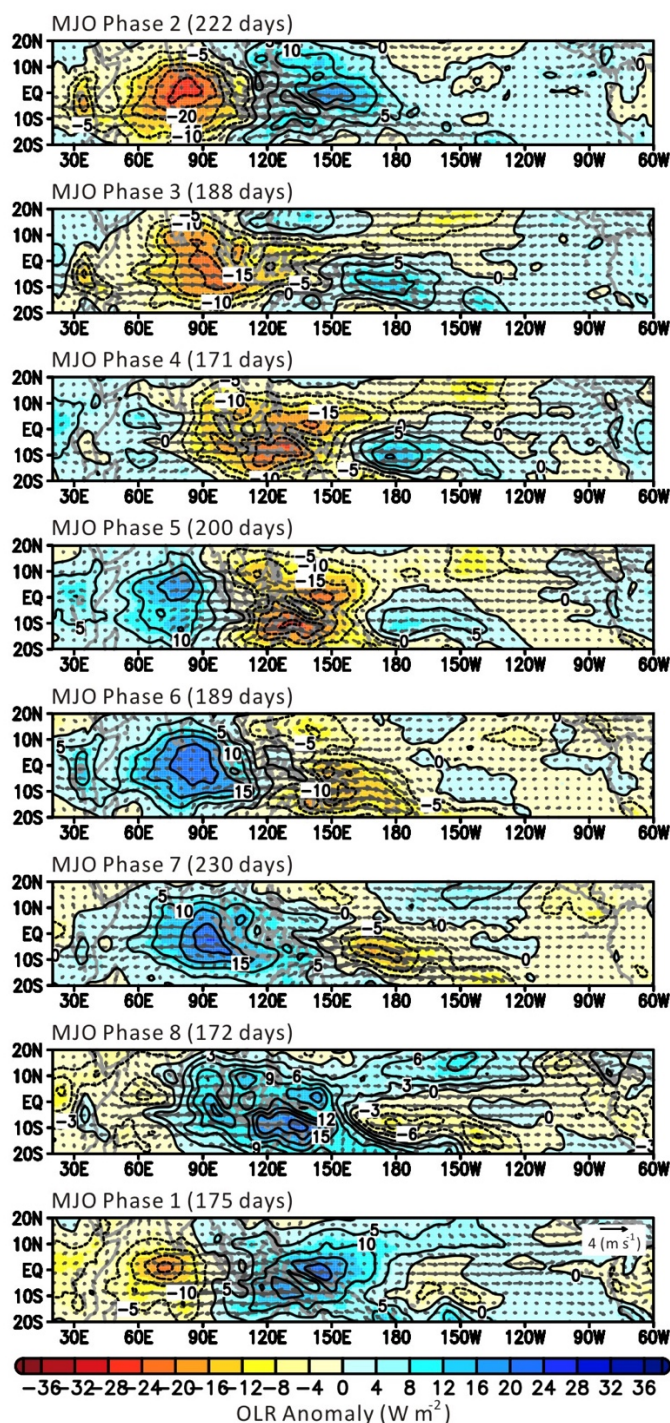
Figure 4: Composites of November to April 20-100 day band-pass filtered NOAA Interpolated Outgoing Longwave Radiation anomalies (color shades and contours, W m⁻²) and horizontal wind anomalies (vectors, m s⁻¹) at 850mb from ERA-Interim, as a function of the eight phases of the MJO (Wheeler and Hendon 2004). Number of days for composites are indicated on the top of each panel. Years of analysis are from 1997 to 2012.

555
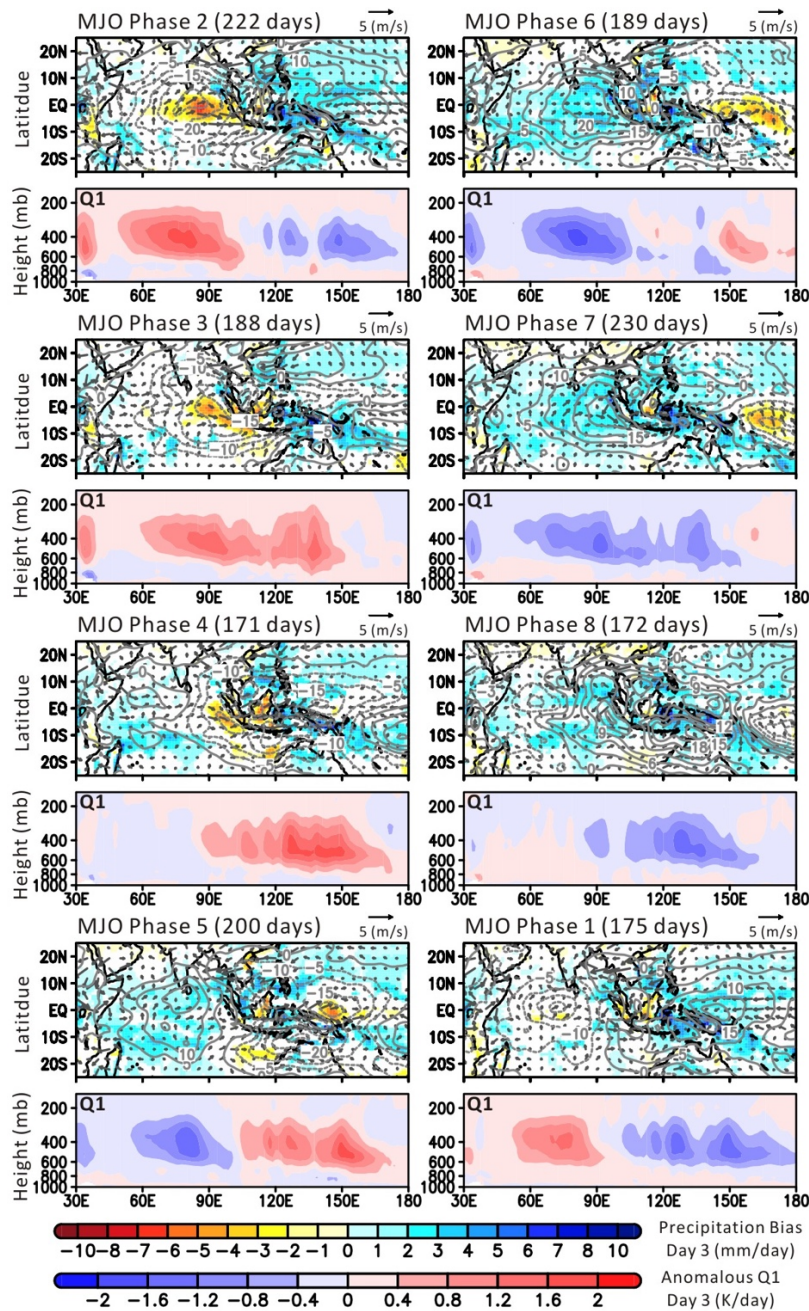
Figure 5: Composites of November to April precipitation bias (color shades, mm day⁻¹), 850 mb horizontal wind biases (vectors, m s⁻¹), and anomalous 20-100 day band-pass filtered Q1 vertical profiles (averaged over 10ºS to 10ºN, K day⁻¹) from Day 3 hindcasts, as well as the 20-100 day band-pass filtered NOAA Interpolated Outgoing Longwave Radiation anomalies (contours, W m⁻²), as a function of the eight phases of the MJO (Wheeler and Hendon 2004). The number of days comprising each composite are indicated on the top of each panel. The observed precipitation and winds are from GPCP and ERA-Interim, respectively. Only precipitation biases that are significant at the 95% confidence level are shaded. The Q1 profiles are computed directly from model's tendency terms with all the diabatic processes.
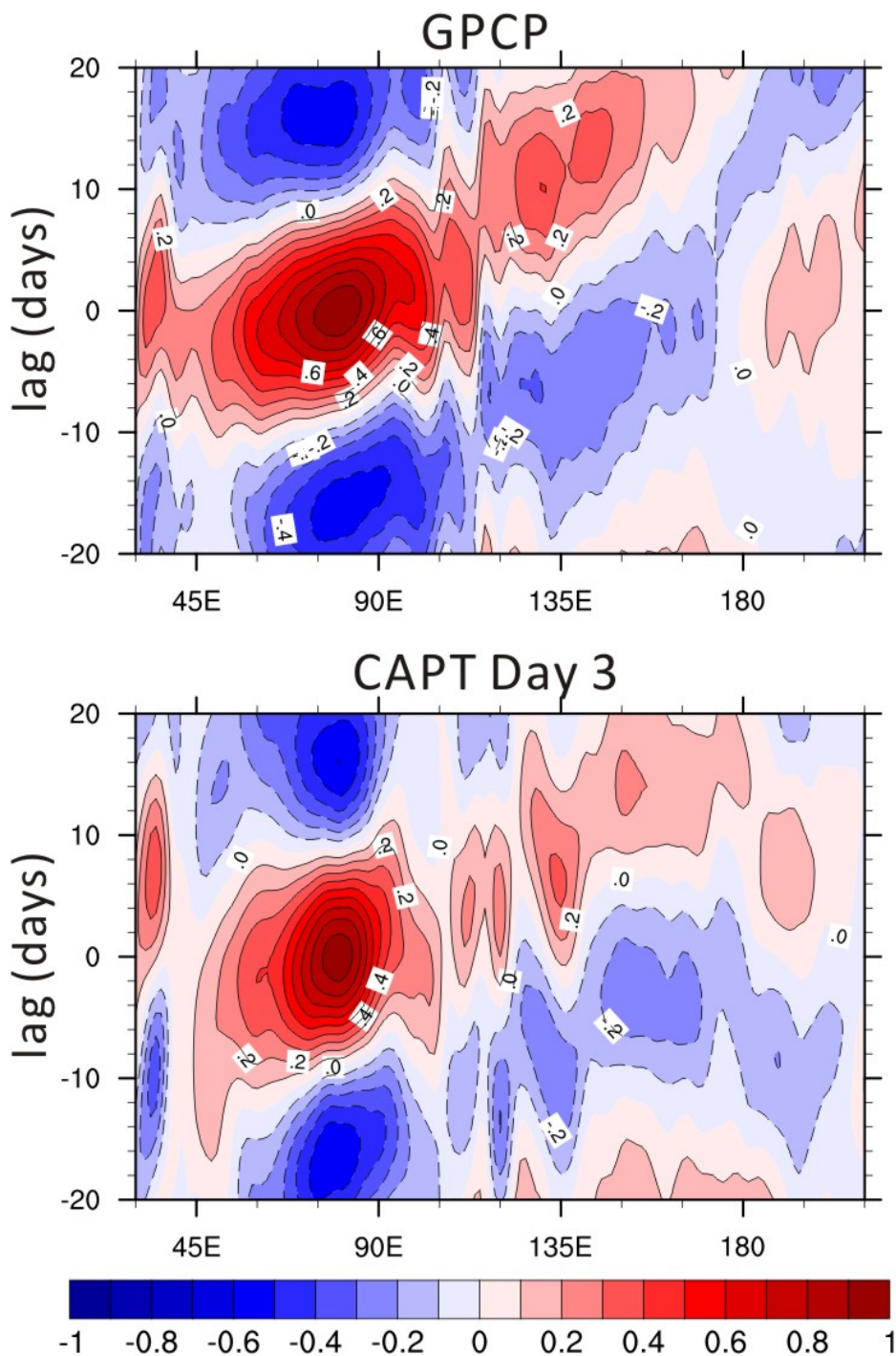
565

Figure 6: Time-longitude anomalous rainfall correlation Homvöller diagram along the Equator (10ºS - 10ºN) based on GPCP and CAPT Day3 hindcasts. The rainfall anomalies associated with the MJO are derived based on lag-correlation over an Indian Ocean box (75º-85ºE; 5ºS-5ºN) for northern winter (November-April) of 1997 to 2012.
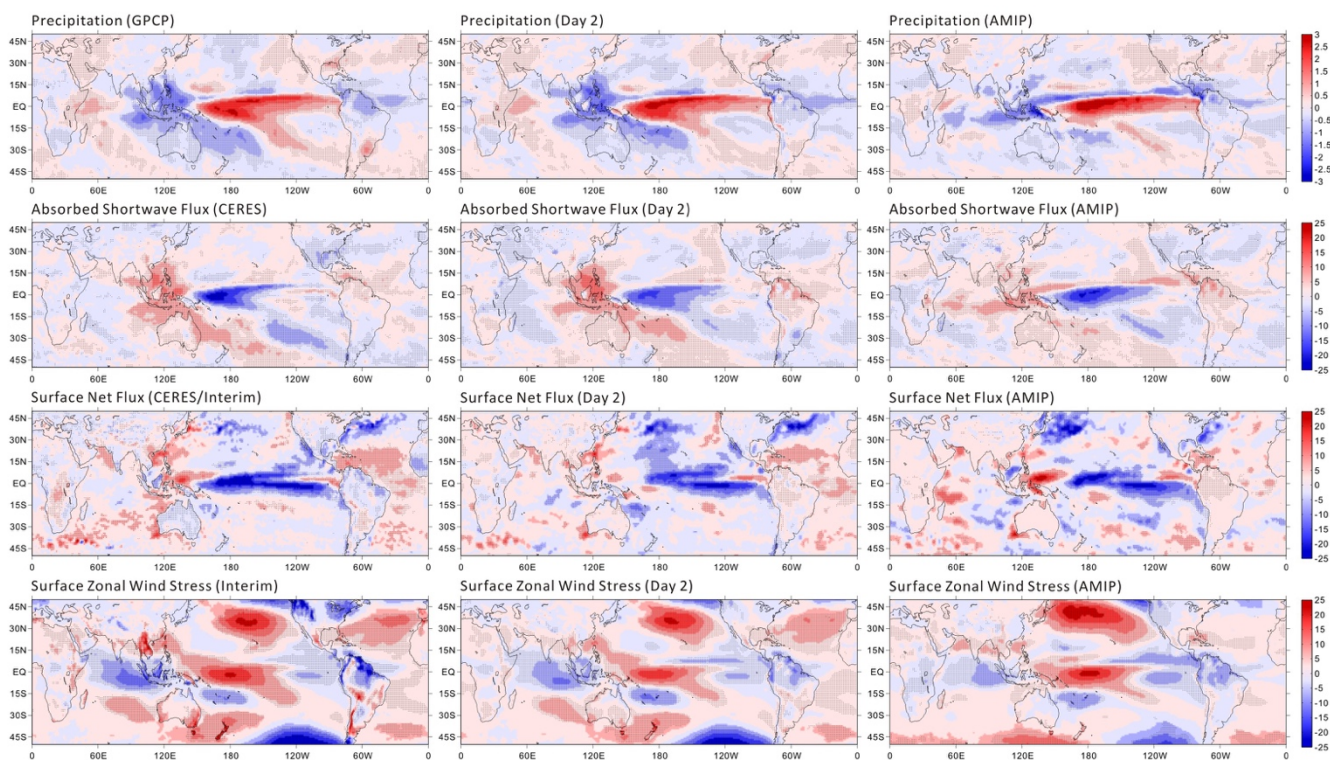
570 **Figure 7: Regression maps of precipitation (mm day⁻¹ K⁻¹), absorbed shortwave radiation (W m⁻¹ K⁻¹), net surface heat flux (W m⁻¹ K⁻¹), surface zonal wind stress (N m⁻² K⁻¹) onto the Niño 3.4 index from observations (left panels), Day 2 hindcasts (middle panels), and AMIP simulation (right panels).**

575
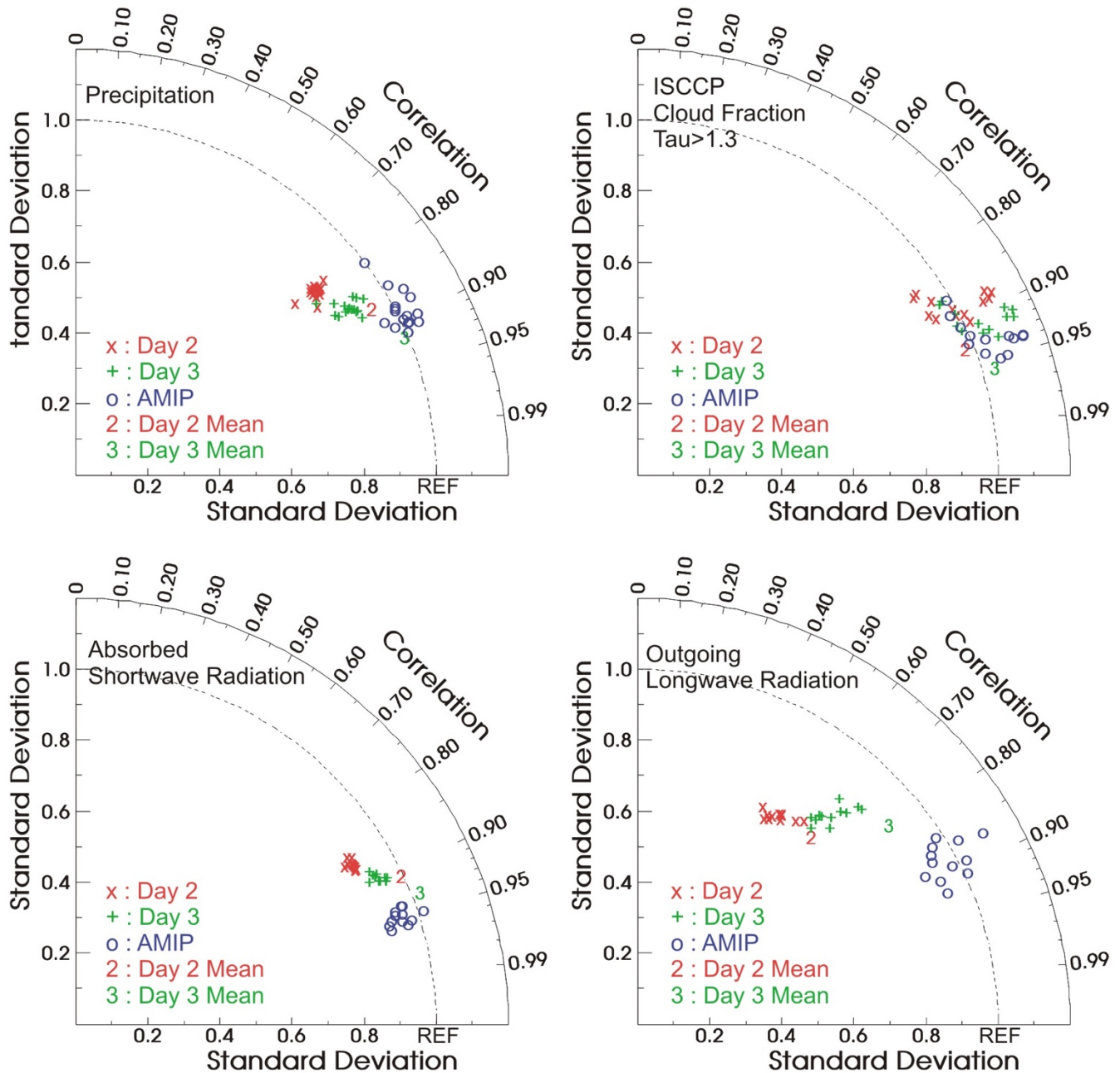
Figure 8: Spatial pattern statistics of the bias errors (with respect to observations) of annual mean precipitation, ISCCP total cloud fraction (with tau > 1.3), absorbed shortwave radiation, and outgoing longwave radiation from the multi-year CAM5 hindcasts and an AMIP simulation. These statistics are illustrated with a Taylor diagram (Tayler et al. 2001) that shows the level of agreement of a given field to a common reference. The reference fields (REF) are the correspondent multi-year mean bias errors from the AMIP simulation. Each "x", "+", or "o" represents the Day 2, Day 3 or AMIP annual mean bias for individual years between 1997 and 2012 whenever the observations are available, and "2" and "3" represents the Day 2 and Day 3 hindcast mean biases averaged over all available years, respectively.
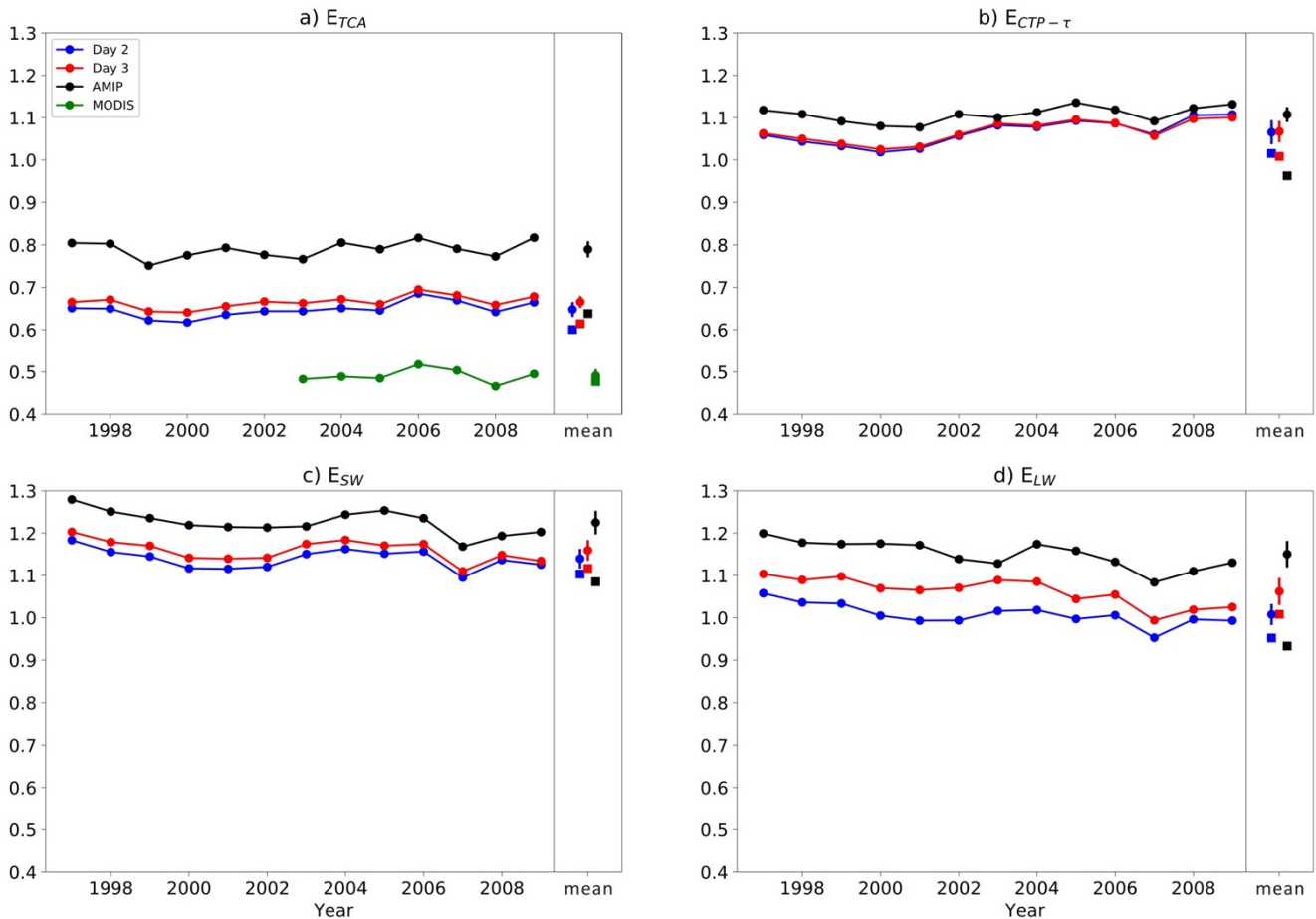
Figure 9: Cloud metrics as defined using the ISCCP simulator in Klein et al. (2013) for Day 2 and 3 hindcasts, as well as the AMIP simulation. These metrics are scalar measures of performance in simulating the space-time distribution of several cloud measures, with better performance indicated by smaller E values. E_{TCA} measures total cloud amount, and $E_{CTP-\tau}$ measures cloud-top pressure and optical depth in different categories of optically intermediate and thick clouds at high, middle, and low-levels of the atmosphere. E_{SW} and E_{LW} measure the impacts on top-of-atmosphere shortwave and longwave radiation in the same categories used for $E_{CTP-\tau}$, respectively. The markers with errorbars show the average and 1-σ interannual variation in these error metrics. The square symbols are the error metrics computed by comparing model and observed monthly-resolved climatological means. MODIS cloud amount for E_{TCA} is plotted as a measure of observational uncertainty.
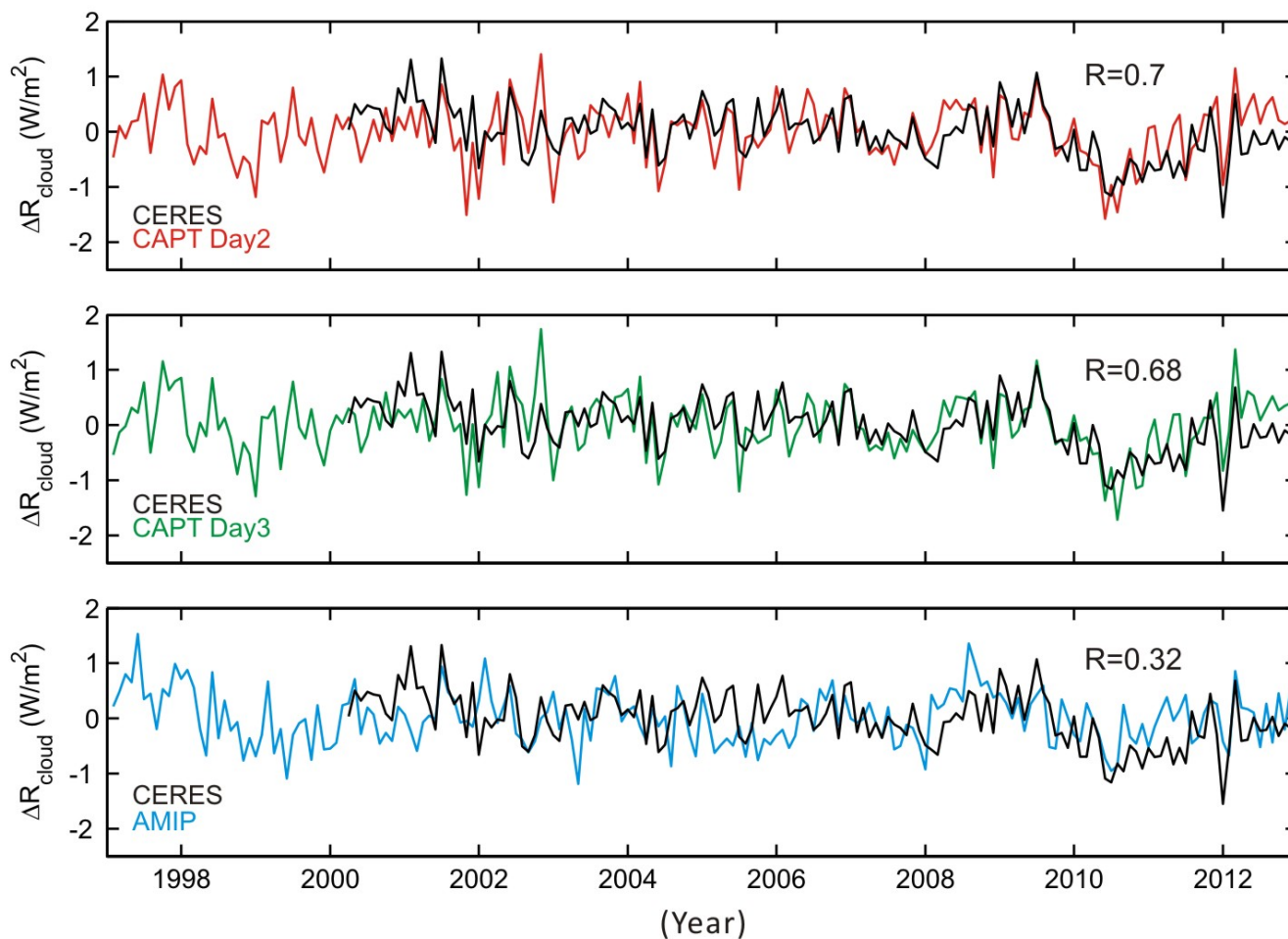
Figure 10: Time series of monthly anomalies of global mean cloud radiative effect from CERES, Day 2 and 3 hindcasts, as well as from the AMIP simulation. The correlation coefficient between the model and observation is shown in the upper right portion of each panel.